

# Microscopic and Macroscopic Bipolar Injection and Carrier Recombination in Single-layer Si Nanocrystals

Jie Xu<sup>1,\*</sup>, Shulin Zheng<sup>1</sup>, Yuxing Chen<sup>1</sup>, Wei Li<sup>2</sup> and Jun Xu<sup>2</sup>

<sup>1</sup> College of Electronic and Optical Engineering, College of Microelectronics, Nanjing University of Posts and Telecommunications, Nanjing 210023, China

<sup>2</sup> National Laboratory of Solid State Microstructures, School of Electronic Science and Engineering, Nanjing University, Nanjing 210093, China

\*jiexu@njupt.edu.cn

**Abstract.** Si nanocrystals (NCs) based optoelectronic devices have attracted more and more attentions due to the quasi-direct energy band structure and the adjustable band gap of Si NCs. In these optoelectronic devices, the carrier injection and recombination process is a crucial issue and needs to be deeply understood. Here, bipolar carrier injection and recombination process in a single layer of Si NCs was observed at the microscopic and macroscopic scales, by electrostatic force microscopy (EFM) and alternating-current electroluminescence (ac EL) measurement, respectively. EFM result showed that opposite charges could be injected into the single-layer Si NCs and they would laterally recombine with each other. On the other hand, the single-layer Si NCs also showed a frequency dependent EL intensity, which was attributed to the time limitation of carrier injection and radiative recombination process.

## 1. Introduction

Bulk Si has an indirect band gap structure that strongly limits its optoelectronic application. However, thanks to the quantum confinement effect, a quasi-direct band structure and size dependent band gap can be expected in Si nanocrystals (NCs), which facilitates the preparation and application of Si NCs-based light emitting diodes (LEDs) and other optoelectronic devices [1-4]. In these devices, carrier injection and recombination process determines the device performance and needs to be deeply studied and understood [5]. In recent years, electrostatic force microscopy (EFM) and Kelvin-probe force microscopy (KFM) have been extensively introduced to visualize the charge injection and spread process in Si NCs based materials, giving detailed information at the nanoscale [6-8]. More recently, we have demonstrated the quantitative relationship between the EFM/KFM signal and sample surface potential, enabling quantitative analysis of surface charge distribution from the microscopy signals [9, 10]. On the other hand, alternating-current electroluminescence (ac EL) detection has been proposed as a powerful tool to observe the radiative recombination process at the macroscopic scale, and even found helpful to enhance the optoelectronic device performance [11, 12]. In the present work, the carrier transportation process of single-layer Si NCs was observed by EFM and ac EL measurement, from which the bipolar injection and recombination behaviors were clearly shown at the microscopic and macroscopic scales respectively.

## 2. Experiments



Content from this work may be used under the terms of the [Creative Commons Attribution 3.0 licence](https://creativecommons.org/licenses/by/3.0/). Any further distribution of this work must maintain attribution to the author(s) and the title of the work, journal citation and DOI.

### 2.1. Sample Preparation

Single-layer Si NCs sandwiched by amorphous Si carbide (a-SiC) layers were prepared by excimer laser crystallization technique [13]. First, a-SiC/a-Si/a-SiC sandwiched structures were deposited on p-Si (100) substrate ( $1.5\text{--}3\ \Omega\text{-cm}$ ) by a conventional plasma enhanced chemical vapor deposition (PECVD) system. Silane ( $\text{SiH}_4$ ) was used for a-Si growth while methane ( $\text{CH}_4$ ) and  $\text{SiH}_4$  ( $[\text{CH}_4]:[\text{SiH}_4]=10:1$ ) gases for a-SiC growth. The thickness of bottom a-SiC and a-Si layers was 10 nm and 4 nm, while that of top a-Si layer was 2 nm (sample A) or 35 nm (sample B). After PECVD growth, both samples were exposed under a KrF excimer laser (Coherent, COMPexPro 201F, 248 nm) to crystallize the a-Si layer and form Si NCs. Finally, plane aluminum electrode was evaporated on the backside of substrate of both samples, and transparent circular indium-tin-oxide (ITO) electrode with a diameter of 1.5 mm was sputtered on the top of sample B. The sample structures are shown in figure 1. In the following experiment, sample A was used for the EFM measurement, and sample B for the ac EL detection.

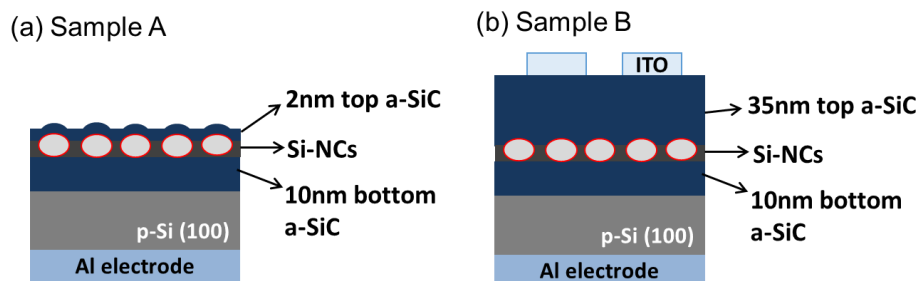


**Figure 1.** The sample structure of (a) sample A and (b) sample B.

### 2.2. EFM Measurement

EFM measurement (Bruker, Nanoscope IIID multimode) was then carried out for sample A to visualize the carrier injection and recombination process. Excess carriers were first injected into Si NCs from the biased conductive tip (Bruker, SCM-PIT type) in a modified tapping mode, where "TM Deflection" parameter was used for feedback control instead of "Amplitude Setpoint" [5], as shown in figure 2(a). The tip scanning rate is 1 Hz per line during the charge injection operation. After charge injection, EFM measurement was implemented in a two-pass interleave scan. In the first pass, the tip scanned the sample surface to obtain topography lines; in the second pass, the tip was lifted 50 nm above the sample surface under a constant bias of +4 V, and finally the tip resonant frequency shift was output as EFM signal, as shown in figure 2(b).

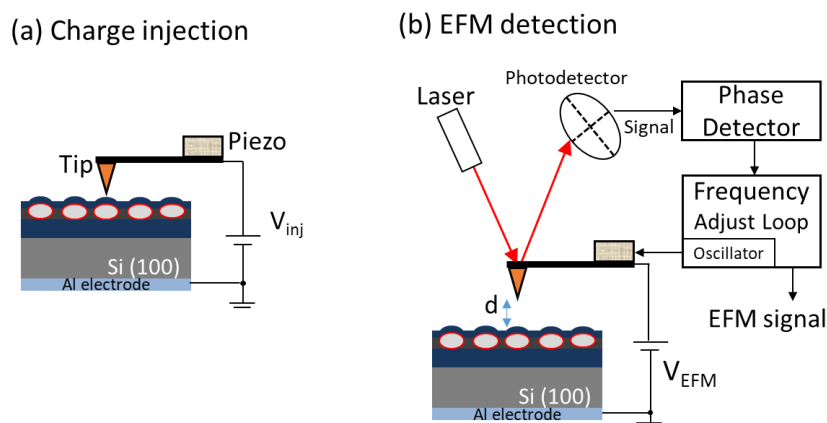


**Figure 2.** (a) The microscopic charge injection operation through a biased tip. (b) EFM measurement in non-contact mode.

### 2.3. AC EL Measurement

Sample B was driven by a sine ac voltage source ( $V_{pp}=14V$ ) that was generated by a source signal generator (Agilent 33210A) connecting to a signal amplifier (Agilent 33502A). The ac EL signal was detected by a CCD detector (HORIBA Jobin Yvon) in the visible range. The EL spectra was calibrated considering the sensitivity of the detector system.

## 3. Results and discussion

### 3.1. Sample structure

Figure 3 shows the atomic force microscopy (AFM) images of sample A before and after excimer laser irradiation. It is shown that the as deposited sample has a smooth surface (rms roughness smaller than 0.2 nm), while after laser annealing, grain-like Si NCs form and they make the surface textured (rms roughness about 1 nm).

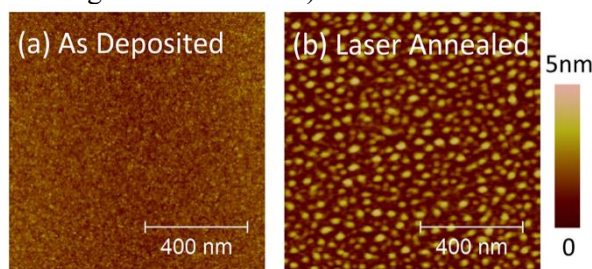


**Figure 3.** AFM topography of sample A (a) before and (b) after excimer laser irradiation.

Moreover, Raman spectrum also proves the crystallization of a-Si layer (not shown here). The as deposited sample only shows an amorphous band around  $480\text{ cm}^{-1}$ , however, after laser annealing a nanocrystalline peak at  $515\text{ cm}^{-1}$  appears which confirms the formation of Si NCs [14].

### 3.2. EFM Results

Figure 4 shows the EFM results after bipolar injection through the biased tip. In figure 4(a), a square area of  $1.5 \times 1.5\text{ }\mu\text{m}^2$  was first charged under  $-3\text{ V}$  tip bias, and then the inner square area of  $0.3 \times 0.3\text{ }\mu\text{m}^2$  was recharged under  $+3\text{ V}$  tip bias. It is shown that the EFM signal  $\Delta f$  reduces in the negatively charged area while it increases in the positive one. Considering that the EFM voltage  $V_{\text{EFM}}$  is positive ( $+4\text{ V}$ ) in the measurement, and that  $\Delta f$  is proportional to the product of  $V_{\text{EFM}}$  and the excess charge quantity [6, 10], it can be deduced that electrons were injected into Si NCs during the  $-3\text{ V}$  injection procedure, and opposite charges (holes) were injected during the following  $+3\text{ V}$  injection process.

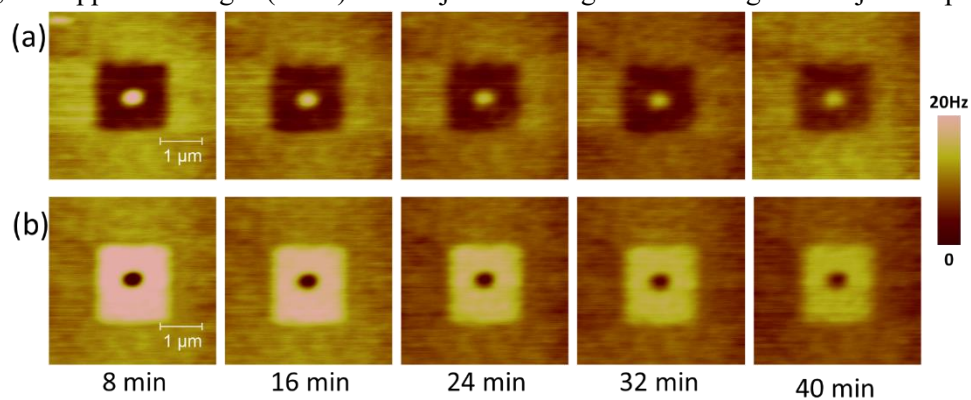


**Figure 4.** EFM images of sample A after bipolar injection. (a) First  $-3\text{ V}$  injection in the  $1.5 \times 1.5\text{ }\mu\text{m}^2$  area and then  $+3\text{ V}$  injection in the inside  $0.3 \times 0.3\text{ }\mu\text{m}^2$  area. (b) Reversed bias polarity compared to (a).  $V_{\text{EFM}}$  equals to  $+4\text{ V}$  in all the images.

It should be noticed here that although the injection bias intensity (3 V) and nominal tip scanning rate (1 Hz per line) are the same, the latter recharging area is much smaller and thus the actual charging scan rate per length is only one fifth of the former charging process, making it possible for electron extraction and hole injection. Figure 4(b) shows a similar result when the injection bias polarity is reversed. The EFM images clearly show the bipolar injection into Si NCs and the opposite-type carriers form a core-ring shape distribution.

The profiles of figure 4 at different elapsed times are plotted in figure 5(a) and (b). It is found that the EFM signal intensity of charged regions gradually decreases to the uncharged level, indicating that there exists charge leakage in the Si NCs. A possible charge leakage channel is through the bottom a-SiC layer to the substrate, which was pointed out by our previous work [5]. Besides, the signal decay is much faster in the charged core area than the surrounding ring area, in both figure 5(a) and (b). The central carriers (holes in figure 5(a) or electrons in figure 5(b)) almost disappear after 40 min, however, the surrounding electrons in figure 5(a) or holes in figure 5(b) still remain about one half after the same period. This phenomenon indicates that in addition to vertical charge leakage through the bottom a-SiC layer to substrate, lateral charge movement and recombination occurred after bipolar injection into Si NCs, shown in figure 5(c). First, the surrounding carriers move to the core due to Coulomb attractive interaction; then, opposite carriers recombine with each other which accelerates the EFM signal decay of the core area. The recombination mechanism may be radiative, non-radiative or even Auger recombination, and the EL detection below shows that radiative recombination is possible in the single-layer Si NCs.

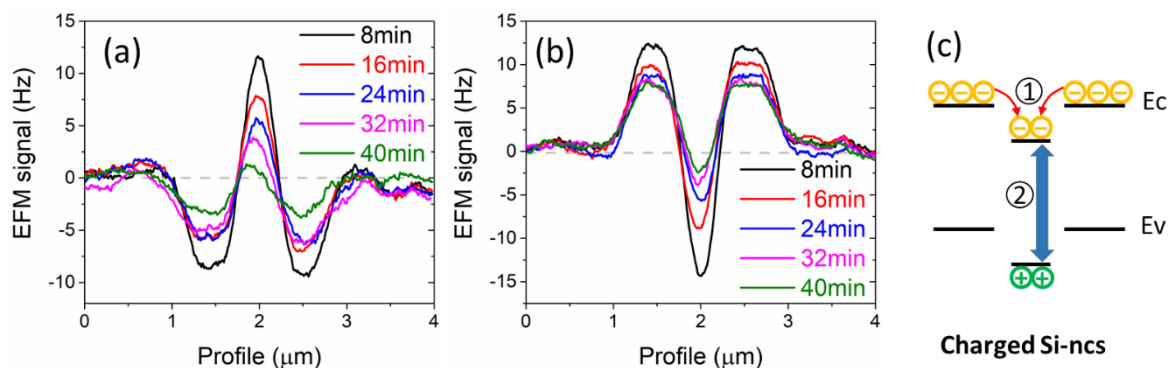


**Figure 5.** (a) The cross-sectional profiles of figure 4(a) at different times. (b) The profiles of figure 4(b). (c) The energy band diagram of Si NCs in figure 4(a), and the carrier movement includes ① the lateral transportation and ② carrier recombination.

### 3.3 AC EL results

EFM measurement shows at the microscopic scale that both electrons and holes can be injected into Si NCs simultaneously, and the carriers will move towards and recombine with each other even when they stay at separate NCs at first. In order to further study the carrier recombination mechanism, EL detection is carried out and it is interesting to discuss the EL spectra under ac drive voltages.

The ac EL spectra of sample B driven by ac voltage sources at different frequencies are shown in figure 6(a). The ac EL spectra shape is very similar to the dc EL spectrum of Si NCs/a-SiC system [14], indicating that they have similar bipolar carrier injection and recombination mechanism. The spectra has a wide band in the visible range, which possibly comes from the radiative recombination of electron-hole pairs in the Si NCs. The photon energy at the peak wavelength (730 nm) is 1.70 eV, which is close to the band-to-band energy for Si NCs embedded in SiC matrix with a diameter of 4 nm [14], and the certain size distribution makes the luminescence peak expanded to a wide band. It is also worth noting here that the EL spectra could only obtained in the forward bias condition (positive bias applied to the p-Si substrate), implying that holes and electrons are injected from the substrate and

ITO electrode respectively. On the other hand, the infrared emission may come from the radiative recombination from Si NCs/a-SiC interface state or band tail states of a-SiC [5].

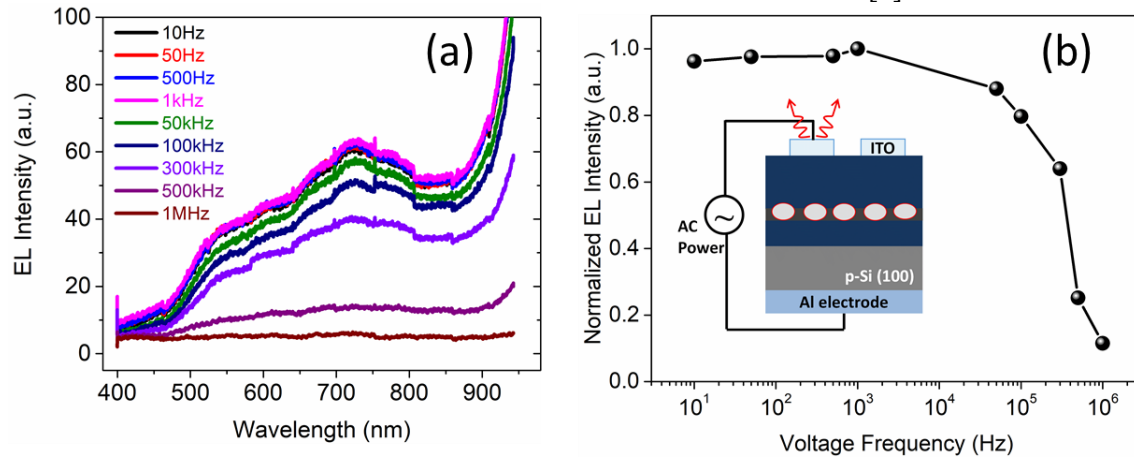


**Figure 6.** (a) The ac EL spectra of sample B at different drive frequencies. The peak to peak voltage  $V_{pp}$  is 14 V. (b) Normalized ac EL intensity at different drive frequencies. The inset is the detection configuration.

Figure 6(b) shows that the EL intensity is dependent on the drive frequency. The EL intensity and shape barely change when the drive frequency increases from 10 Hz to 1 kHz, however, the EL intensity gradually decreases when the drive frequency reaches 50 kHz and it totally disappears at 1 MHz. The recombination mechanism is thought unchanged at different drive frequencies, but under high frequency voltage conditions the carriers do not have enough time to tunnel through the a-SiC layer into Si NCs. Besides, the radiative recombination lifetime of Si NCs is about several microseconds [15], and thus the bias at high drive frequency will also extract the injected carriers and drop their recombination chance. Therefore, it can be deduced that the time needed for carriers injection and recombination process of our sample is about 20  $\mu$ s (1/50 kHz), which is consistent with the time-resolved photoluminescence (TRPL) measurements of Si NCs [16].

Figure 7 shows the supposed energy band diagram of the EL emission process. First, electrons and holes were injected from ITO electrode and substrate, respectively, through Fowler-Nordheim tunneling under a large forward bias. Second, electrons and holes relaxed to the band edge from the high energy state. Finally, electron-hole pairs radiatively recombined with each other and emitted a light band centered at 730 nm. Besides, the infrared light emission might derived from the carrier recombination from interface or band tail states.

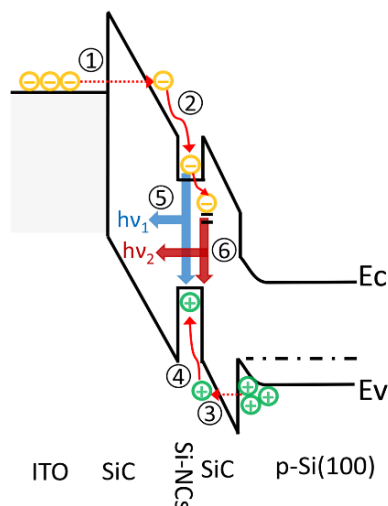


**Figure 7.** The energy band diagram of the bipolar carrier injection and recombination in the single-layer Si NCs. ① ③ : carrier tunneling through the a-SiC layer; ② ④ : carrier relaxation process; ⑤ : visible light emission from band-to-band recombination in Si NCs; ⑥ : infrared light emission from the interface or band tail states.



#### 4. Conclusions

Single-layer Si NCs were prepared by laser crystallization technique. The bipolar injection and carrier recombination process was observed by EFM and ac EL measurement at the microscopic and macroscopic scales, respectively. EFM result shows that electrons and holes can be simultaneously injected into Si NCs by a biased tip in contact with the sample surface. Adjacent opposite charges will attract and recombine with each other due to Coulomb interaction, and it accelerates the charge leakage process. To further study the carrier recombination mechanism, ac EL detection was also carried out. It is shown that electrons and holes will be injected from top electrode and substrate respectively, and finally recombine to emit visible light. The EL intensity gradually diminishes when the drive frequency increases to 50 kHz, which implies a time limitation (about 20  $\mu$ s) needed for the carrier injection and recombination process.

#### Acknowledgements

This work is supported by Natural Science Foundation of Jiangsu Province (No. BK20160909), NUPTSF (Nos. NY215039 and NY217041) and STITP 2018 of NUPT (No. 399). The authors also want to thank Dr. Dongke Li, Dr. Zewen Lin and Dr. Jingjing Liu for their helpful discussions.

#### References

- [1] Maier-Flaig F, Rinck J, Stephan M, Bocksrocker T, Bruns M, Kubel C, Powell A K, Ozin G A and Lemmer U 2013 *Nano Lett.* **13** 475-80
- [2] Priolo F, Gregorkiewicz T, Galli M and Krauss T F 2014 *Nat. Nanotechnol.* **9** 19-32
- [3] Yanagawa H, Inoue A, Sugimoto H, Shioi M and Fujii M 2017 *J. Appl. Phys.* **122** 223101
- [4] Zhang P, Li D K, Jiang L Y and Xu J 2017 *J. Phys.: Conf. Ser.* **844** 012012
- [5] Xu J, Ji Y, Lu P, Bai G, Ren Q and Xu J 2018 *AIP Adv.* **8** 015224
- [6] Mélin T, Diesinger H, Deresmes D and Stiévenard D 2004 *Phys. Rev. Lett.* **92** 166101
- [7] Borowik Ł, Kusiaku K, Deresmes D, Théron D, Diesinger H, Mélin T, Nguyen-Tran T and Roca i Cabarrocas P 2010 *Phys. Rev. B* **82** 073302
- [8] Melitz W, Shen J, Kummel A C and Lee S 2011 *Surf. Sci. Rep.* **66** 1-27
- [9] Xu J, Wu Y, Li W and Xu J 2017 *Nanotechnology* **28** 365705
- [10] Xu J, Chen D, Li W and Xu J 2018 *J. Appl. Phys.* **123** 184301
- [11] Mu W, Zhang P, Xu J, Sun S, Xu J, Li W and Chen K 2014 *IEEE J. Sel. Top. Quant.* **20** 206-11
- [12] Liu J, Sheng X, Wu Y, Li D, Bao J, Ji Y, Lin Z, Xu X, Yu L, Xu J and Chen K 2018 *Adv. Opt. Mater.* **6** 1700897
- [13] Xu J, Xu J, Wang Y, Cao Y, Li W, Yu L and Chen K 2014 *Nanotechnology* **25** 055703
- [14] Rui Y, Li S, Xu J, Cao Y, Li W and Chen K 2012 *J. Non-Cryst. Solids* **358** 2114-7
- [15] Walters R J, Bourianoff G I and Atwater H A 2005 *Nat. Mater.* **4** 143-6
- [16] Lu P, Li D, Zhang P, Tan D, Mu W, Xu J, Li W and Chen K 2016 *Opt. Mater. Express* **6** 3233